Targeting glycolysis in endothelial cells to prevent intraplaque neovascularization and atherogenesis in mice

Perrotta, P.

Chapter 7

[^{18}F]ZCDD083: a PFKFB3 targeted PET tracer for imaging the atherosclerotic plaque

De Dominicis C, **Perrotta P**, Dall'Angelo S, Wyffels L, Staelens S, De Meyer GRY, Matteo Zanda M.

ACS Medicinal Chemistry Letters.2020;11:933-939

Abstract

An emerging target for diagnosis and therapy of atherosclerosis is PFKFB3, a glycolysis-related enzyme up-regulated in inflammatory conditions and angiogenesis. A tosylated precursor of the phenoxindazole PFKFB3 inhibitor [^{18}F]ZCDD083 was synthesised, radiolabelled in 17 ±5% radiochemical yield and >99% radiochemical purity and formulated for *in vivo* PET imaging. *In vivo* stability analysis showed no significant metabolite formation. Biodistribution studies showed high blood pool activity and slow hepatobiliary clearance. Significant activity was detected in the lung (2 h pi: 11.0 ±1.5 %ID/g), while at 6h pi no pulmonary background was observed. *Ex vivo* autoradiography at 6 h pi showed significant high uptake of [^{18}F]ZCDD083 in arch region and brachiocephalic artery of atherosclerotic mice, and no uptake in control mice. This is consistent with plaques distribution seen by lipid staining along with PFKFB3 expression seen by immunofluorescent staining. *In vivo* PET scans showed higher aortic region uptake of [^{18}F]ZCDD083 in atherosclerotic ApoE$^{-/-}$Fbn1$^{C1039G+/-}$ than control mice (0.78 ± 0.05 vs 0.44 ± 0.09 %ID/g). [^{18}F]ZCDD083 was detected in aortic arch and brachiocephalic artery of ApoE$^{-/-}$ (with moderate atherosclerosis) and ApoE$^{-/-}$Fbn1$^{C1039G+/-}$ (with severe, advanced atherosclerosis) mice, suggesting that it may represent a promising tracer for the non-invasive detection of atherosclerotic plaques

Introduction

Atherosclerosis is a pathological process characterized by progressive accumulation of lipids, inflammatory cells and connective tissue in the arterial wall.[1] This process, leading to the formation of the so-called “atherosclerotic plaques”, is predominantly asymptomatic. However, the progression of the disease can cause progressive stenosis of arterial lumen, which can eventually result in ischemic heart pain. Acute clinical events, such as myocardial infarction, stroke and unstable angina, are mainly associated with instability of plaques and formation of occlusive thrombi.[2] According to World Health Organization (WHO), cardiovascular diseases are the first cause of death worldwide and indeed atherosclerosis is a condition associated with the majority of these diseases.[3,4]

The progression of atherosclerotic plaques is initially asymptomatic, characterized by the slow growth of “silent” stable plaques. The development of fibrous plaques in coronary arteries may lead to stable angina, whereas plaque rupture is associated with unstable angina, acute myocardial infarction (MI), and sudden cardiac death. Similarly, rupture of carotid artery plaque is associated with cerebral ischemic events.[5] The risk of thrombotic complications of atherosclerosis is mostly related to the instability of an atheroma rather than the size of the plaque.

Currently, cardiovascular medicine aims principally to identify atherosclerotic plaques prone to rupture, improve the risk stratification, monitor the disease progression, assess new anti-atherosclerotic therapies and promptly evaluate the efficacy of therapeutic treatment. PET imaging is non-invasive and has a great potential in this context. Indeed, new targets and radiotracers are currently being investigated for imaging unstable atherosclerotic plaque.[6,7]

We have studied PFKFB3 enzyme as a new target to be used for the in vivo assessment of atherosclerotic plaques.[8,9] PFKFB3 is a glycolysis-related enzyme upregulated in inflammatory and hypoxic conditions.[10,11] Several studies have shown a tight correlation between PFKFB3 and angiogenesis, which is a feature of vulnerable atherosclerotic plaques.[12,13,14,15] Here we described the development of a specific PET radiotracer targeting PFKFB3 - the ^{18}F-radiolabelled phenoxindazole ZCDD083 – based on the structure of the potent PFKFB3 inhibitor AZ68 (IC_{50}= 4nM).[16]

Results

Fragment 2 (Scheme 1) was obtained from N-Boc-proline and O-Bn-4-aminophenol which were coupled to afford compound 1 which was debenzylated over Pd.

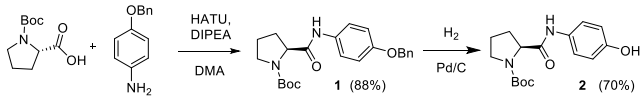

Scheme 1. Synthesis of fragment 2.

Fragment 4 (Scheme 2) was synthesized by NIS-promoted iodination of (2-amino) phenyl-acetonitrile, followed by indazole ring formation via Sandmeyer reaction and intramolecular ring closure of the diazonium salt formed from 3.

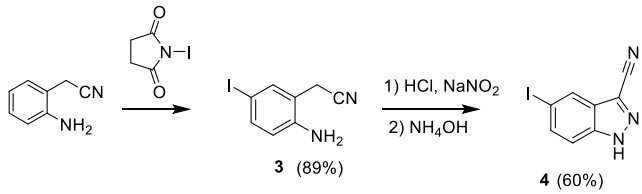

Scheme 2. Synthesis of fragment 4.

The radiofluorination precursor 7 (Scheme 3) was synthesized next. Commercial 2-methyl-1,3-propanediol was then treated with tosyl chloride to give the mono tosylated derivative 5, which was reacted with the indazole 4 via Mitsunobu reaction to give compound 6. Ullmann-type coupling with phenol 4 afforded the target tosylated precursor 7.

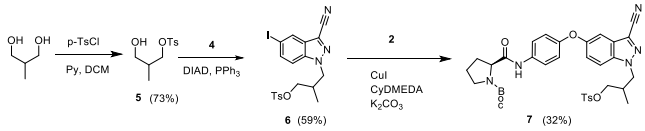

Scheme 3. Synthesis of radiofluorination precursor 7.

The ‘cold’ (e.g. non-radioactive) tracer ZCDD083 (Scheme 4) was prepared from the indazole tosylate 6, which was treated with TBAF to give the fluorinated compound 8. The latter was subjected to the Ullmann coupling affording 9, which was N-Boc-deprotected to afford the target molecule.

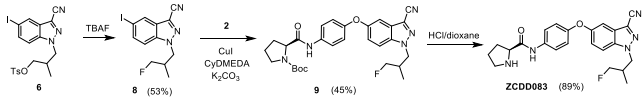

Scheme 4. Synthesis of 'cold' ZCDD083.

Radiosynthesis of [^{18}F]ZCDD083

Starting from the tosylated precursor 7, [^{18}F]ZCDD083 was prepared in a two-step synthesis (Scheme 5) using standard ^{18}F-fluoride chemistry, producing first the protected tracer 10 which was then treated with HCl in order to remove the N-Boc-protection.

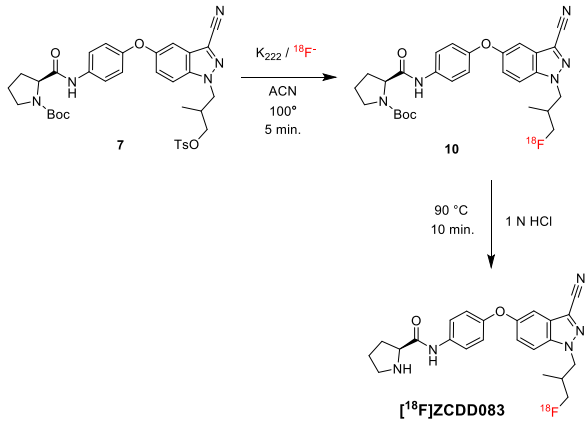

Scheme 5. Radiosynthesis of [^{18}F]ZCDD083.

[^{18}F]ZCDD083 was obtained with a 17 ±5% radiochemical yield (decay-corrected to EOB) and the activity was in the range of 4.7-7.2 GBq (n = 7). The average time taken for synthesis, purification and formulation was 65 minutes. [^{18}F]ZCDD083 was obtained with radiochemical purity >99%, chemical purity >95% and specific activity >130 GBq/μmol (Figure 1).

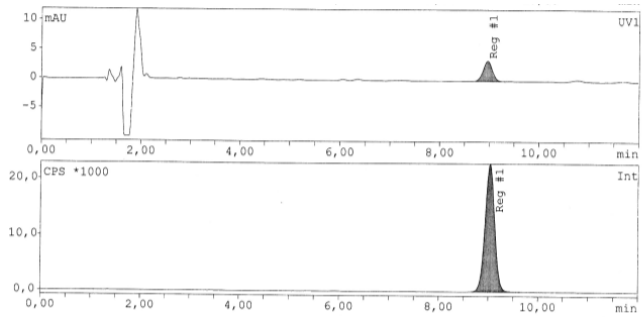

Figure 1. Chemical and radiochemical purity assessed by analytical RP-HPLC. No impurities were detected in the UV (top) and radioactive (bottom) spectra. Column: Phenomenex Luna C18 column (5 µm, 100 Å, 250 × 4.6 mm). Mobile phase: solvent A = H_2O + 0.1% TFA, solvent B = CH_3CN + 0.1% TFA; Isocratic method 40% B.

In vivo stability and ex vivo biodistribution

The radio-HPLC analysis showed no significant metabolite formation within 6 h. The eluate from HPLC was collected in fractions and the radioactivity in each fraction was measured in a γ-counter. At 6 h pi, 78.9% ±1.2 of [^{18}F]ZCDD083 was intact.

The measurement of radioactivity by γ-counter showed a high overall accumulation of [^{18}F]ZCDD083 in tissues and organs within 2 h pi, as shown in Figure 2. More specifically, high blood radioactivity was observed (7.2 ±2.2 %ID/g at 15 min pi, 5.5±1.6 %ID/g at 1 h pi, and 2.1±0.4 %ID/g at 2 h pi), revealing a slow clearance of [^{18}F]ZCDD083 from blood pool. Also, high pulmonary uptake was found (34.7 ± 6.0 %ID/g at 15 min) with a slow washout from lungs (11.0 ± 1.5 %ID/g at 2 h. On the contrary, at 6 h pi the radioactivity in lungs and blood was significantly lower (5.5±3.9 %ID/g and 1.5±1.1 %ID/g respectively).

Instead, at the late time point [^{18}F]ZCDD083 had mostly accumulated in the excretory organs (i.e. 25.5 ± 3.8 %ID/g in small intestine and 47.9 ± 6.4 %ID/g in large intestine). Level of uptake in the liver and the intestines were significantly higher compared to the kidneys. Therefore, it can be concluded that [^{18}F]ZCDD083 is predominantly cleared via the hepatobiliary system into the intestines and that the renal clearance is less significant.

Ex vivo biodistribution evaluation at 6 h pi was carried out also in atherosclerotic ApoE$^{-/-}$ mice. A similar [^{18}F]ZCDD083 biodistribution profile was observed in atherosclerotic ApoE$^{-/-}$ and control C57BL/6J mice. Pharmacokinetic studies in ApoE$^{-/-}$ atherosclerotic mice confirmed a prolonged plasma half-life of [^{18}F]ZCDD083 (1.4 ±0.2 %ID/g in blood).

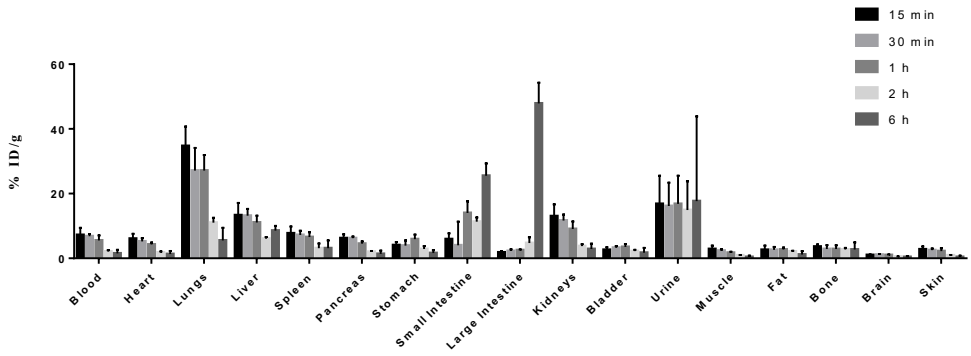

Figure 2. Ex vivo biodistribution of [18F]ZCDD083. Slow blood clearance and high tracer uptake in the lungs were observed at earlier time points within 2 h pi.At 6 h pi [18F]ZCDD083 was mostly accumulated in the intestines.

Residual high radioactivity accumulation was observed in lungs (8.6 ± 1.9 %ID/g), whereas the maximal uptake was found in small and large intestine (40.6 ± 45.8 %ID/g and 35.6 ± 2.3 %ID/g respectively).

PET/CT imaging studies

[^{18}F]ZCDD083 PET imaging scans were performed using two different disease models (ApoE$^{-/-}$ and ApoE$^{-/-}$Fbn1$^{C1039G+/-}$) and aged-matched wild type C57BL/6J mice as controls.

Spherical ROI$_s$ were drawn manually over each aortic arch and ascending aorta using the axial view of CT images. The [^{18}F]ZCDD083 signal was then quantified as SUV_{mean} values. Tracer uptake was significantly different in ApoE$^{-/-}$Fbn1$^{C1039G+/-}$ (SUV 0.78 ± 0.05), ApoE$^{-/-}$ (SUV 0.55 ± 0.06) and C57BL/6J mice (SUV 0.44 ± 0.09), as shown in Figures 3 and 4.

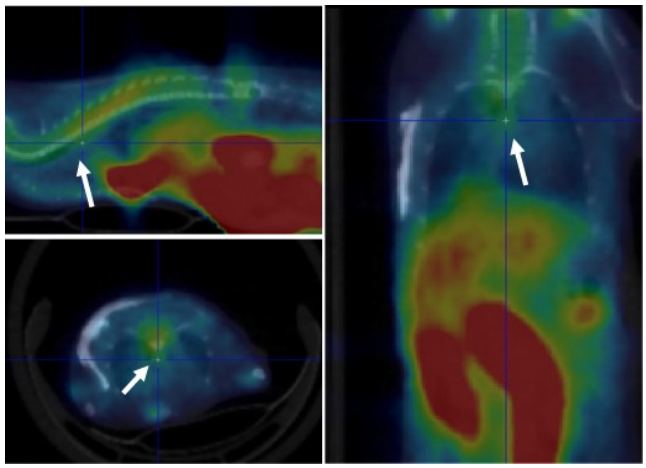

Figure 3. Representative axial, sagittal and coronal views of PET/CT images of ApoE$^{-/-}$ Fbn1$^{C1039G+/-}$acquired at 6 h after injection of [^{18}F]ZCDD083. Radioactive signal in aorta (white arrows) was observed.

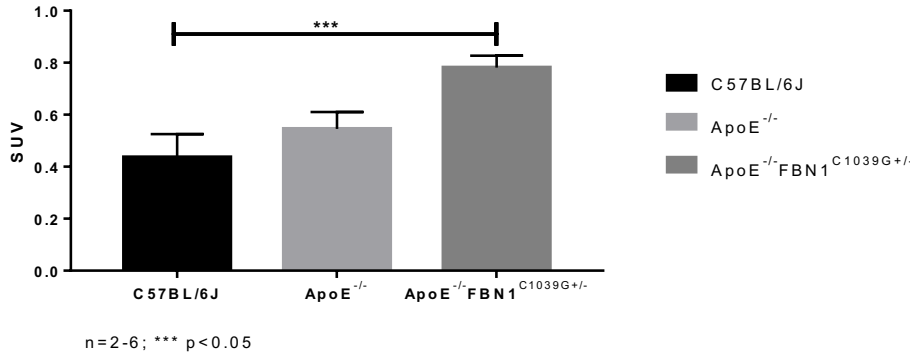

Figure 4. Comparison of SUV measurements in C57BL/6J (n = 6), ApoE$^{-/-}$ (n = 6) and ApoE$^{-/-}$Fbn1 $^{C1039G+/-}$ mice (n = 2). All values are given as mean ± SD. One-way ANOVA was performed to test for difference between groups. One ApoE$^{-/-}$Fbn1$^{C1039G+/-}$ mouse was excluded from the analysis because of a PET image acquisition technicality. (***p = 0.0006, one-way ANOVA followed by Brown-Forsythe test).

Autoradiography and Oil red O staining

At the end of the PET imaging scans, three mice of C57BL/6J, ApoE$^{-/-}$ and ApoE$^{-/-}$ Fbn1$^{C1039G+/-}$ were sacrificed and the aorta was harvested for Red Oil O staining and autoradiography (ARG). The ex vivo distribution of atherosclerotic plaques within the aorta was assessed by Red Oil O staining, whereas the accumulation of [^{18}F]ZCDD083 was assessed by autoradiography of the in vivo injected [^{18}F]ZCDD083. Oil This aforementioned Red O staining and ex vivo autoradiography were performed on the same aortic specimens in order to visually compare fat-stained areas and tracer distribution within the aorta (Figure 5).

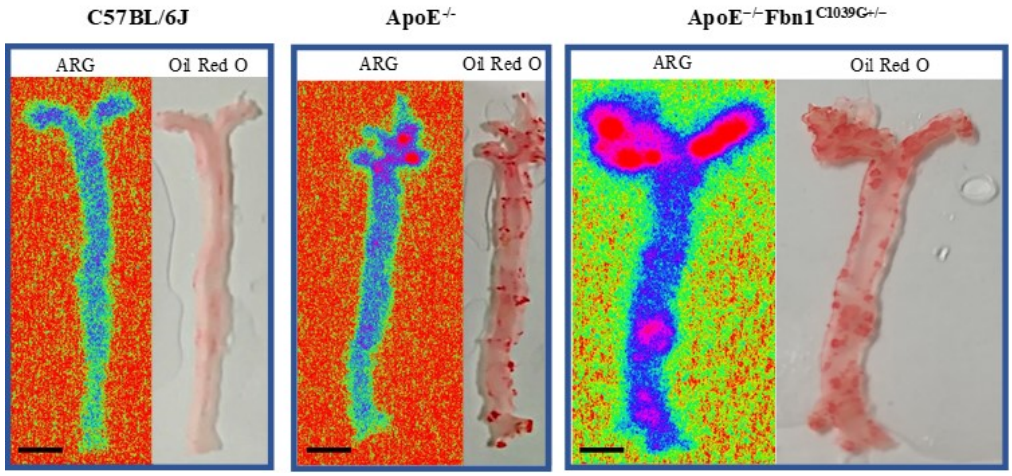

Figure 5. [^{18}F]ZCDD083 aortic uptake vs plaque distribution. Ex vivo autoradiography (left) and fat staining using Oil-red O (right) of longitudinally opened aortas at 6h post injection of [^{18}F]ZCDD083 in C57BL/6J control mice compared to atherosclerotic mice (ApoE$^{-/-}$ and ApoE$^{-/-}$Fbn1$^{C1039G+/-}$). [^{18}F]ZCDD083 uptake colocalises with atherosclerotic plaques. Scale bar = 1 cm.

Aortas from C57BL/6J control mice did not show focal lipid stained areas and radioactivity signal. Conversely, atherosclerotic plaques were found in ApoE$^{-/-}$ mice, especially in the aortic arch, proximal aorta and brachiocephalic aorta. The Oil Red O staining showed also a low plaque load in the thoracic descending aorta of the ApoE$^{-/-}$ strain. The ARG of the same specimen showed that the tracer accumulation within the aorta matched exactly with the distribution of atherosclerotic lesions. More specifically, the radioactivity was accumulated mostly in the aortic arch and in the branches. In these regions the [^{18}F]ZCDD083 uptake was significantly higher in ApoE$^{-/-}$ (0.022 ± 0.004 %ID/μL) than control mice (0.011 ± 0.003 %ID/μL) ($p = 0.0378$, unpaired t test).

The correlation between plaques and tracer uptake was also consistent using ApoE$^{-/-}$Fbn1$^{C1039G+/-}$ mice with higher plaque load than the ApoE$^{-/-}$ strain . The comparison of corresponding en face lipid staining and autoradiographic signals demonstrated a high correlation of fat-stained areas and radioactivity distribution. ApoE$^{-/-}$Fbn1$^{C1039G+/-}$ mice showed more extended atherosclerotic lesions in the arch

region, brachiocephalic artery along with thoracic descending aorta. [^{18}F]ZCDD083 was, indeed, detected in the same areas along the aorta.

Histology and immunohistochemistry

Aortic specimens of C57BL/6J and ApoE$^{-/-}$ (n = 3/ each group) were used for further histological analysis after PET imaging studies. Longitudinal sections of aortic arch and right common carotid artery as well as cross sections of brachiocephalic aorta and proximal aorta were stained with hematoxylin and eosin (H&E) to visualize atherosclerotic plaques and lesion morphology. Aortas of healthy mice did not show atherosclerosis, whereas ApoE$^{-/-}$ mice showed fibrous/atheromatous plaques and some small calcifications. The H&E staining confirmed atherosclerotic disease especially in brachiocephalic artery, proximal aorta and aortic arch.
The immunohistochemistry of ApoE$^{-/-}$ aortic arch sections, revealed that the enzyme target PFKFB3 is overexpressed inside atherosclerotic plaques (Figure 6).

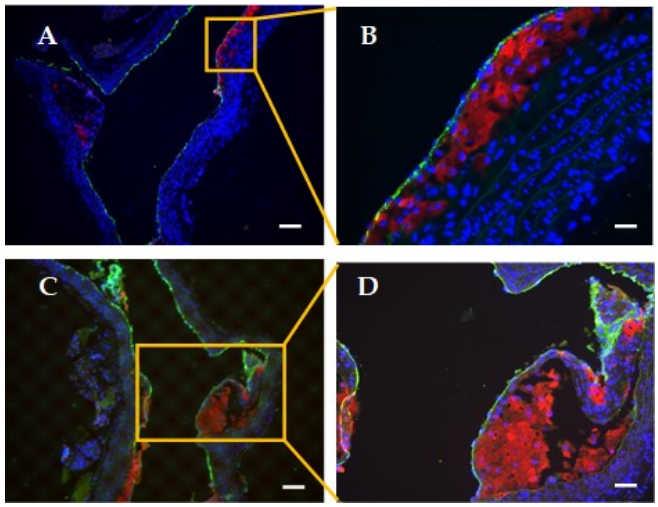

Figure 6. Immunohistochemistry of the aorta from ApoE$^{-/-}$ mice. Two longitudinal sections of the aortic arch are shown (A, C) as well as a high-power magnification (B, D). Endothelial cells are stained using von Willebrand factor (green). Nuclei (blue) are counter-stained with DAPI. Positive staining areas for PFKFB3 (red) are observed inside atherosclerotic plaques. Scale bar = 100 μm (A, C); 20 μm (B); 50μm (D).

The comparison among brachiocephalic arteries of atherosclerotic and control mice showed that PFKFB3 was highly expressed within atherosclerotic plaques, whereas in normal vessels PFKFB3 is present just in a basal level along the arterial wall (Figure 7).

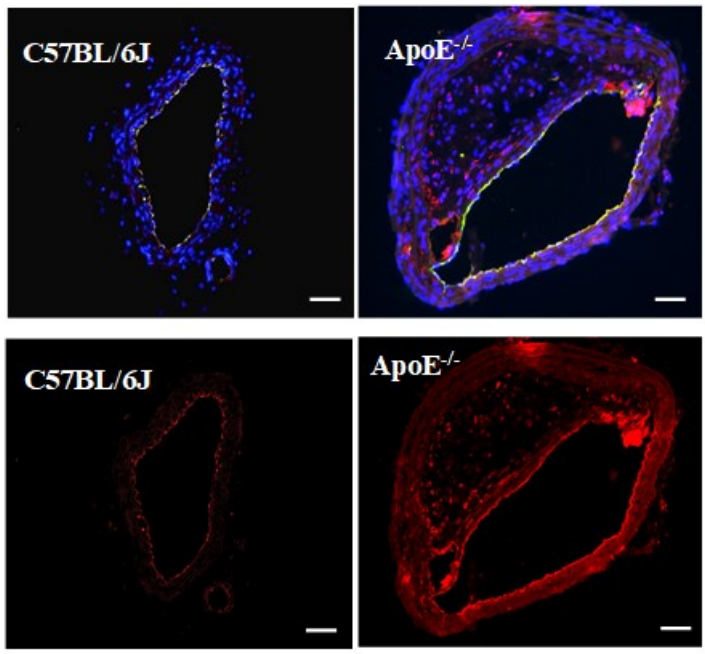

Figure 7. Immunohistochemistry of murine brachiocephalic arteries. Upper panels: immunofluorescent staining for von Willebrand factor to detect endothelial cells (green) and PFKFB3 (red). Counter-staining with DAPI to detect nuclei (blue). Lower panels = PFKFB3 staining (red). ApoE$^{-/-}$ mice exhibit high expression level of PFKFB3 enzyme in contrast to C57BL/6J controls. Scale bar = 50 µm.

Discussion

Atherosclerosis is responsible for the majority of acute cardiovascular events. Specifically, rupture of atherosclerotic plaques and consequent thrombosis remains the largest underlying cause of cardio- and cerebrovascular death. Despite extraordinary advances in the understanding of the pathophysiology of atherosclerosis, both the diagnosis and treatment of the disease still present limitations. Currently, the main challenge in cardiovascular medicine is to identify patients who are at risk of coronary plaque rupture and subsequent heart attack or stroke originating from carotid plaque depoistions.[17] Among the cardiovascular imaging modalities used, coronary angiography has a wide clinical application but provides information only on vessel stenosis. Other imaging techniques, such as intravascular ultrasound (IVUS), optical coherence tomography (OCT) and near-infrared spectroscopy (NIRS), can provide only a limited plaque characterization but, unfortunately, they are invasive and thus not useful for patient diagnosis and follow up.[18,19,20] Therefore, new non-invasive approaches to detect potentially unstable plaque are urgently needed.

In this context, positron emission tomography (PET) imaging has great potential, since - compared to other molecular imaging modalities - it shows higher sensitivity allowing better visualization of biological and biochemical processes involved in the development of atherosclerotic plaques.[21] Among the PET radiotracers currently available, only ^{18}F-FDG has been approved for clinical use. In particular, clinical studies showed that ^{18}F-FDG is useful to assess carotid artery stenosis in asymptomatic patients.[22,23] However, carotid artery imaging using ^{18}F-FDG PET is challenging due to (1) the low spatial resolution of PET (≈ 4 mm in human PET and 1,2 mm in rodent PET), (2) cardiac motion and (3) myocardial spill over.[24] To address the latter limitation, new imaging targets and radiotracers having lower unspecific myocardial uptake are currently under investigation.[25]

The results above validate PFKFB3 enzyme as an imaging target of atherosclerosis in two mouse models.[26,27] Firstly, we observed an increased target engagement in cross sections of diseased aortas of atherosclerotic mice compared to those of healthy mice. Secondly, longitudinal sections of aortic arch specimens of ApoE$^{-/-}$ mice showed higher expression level of PFKFB3 enzyme within atherosclerotic

plaques compared to normal vessel wall. Hence, all these results demonstrated the appropriateness and the specificity of the target PFKFB3 for the detection of atherosclerotic plaques.

Once we demonstrated the relevance of PFKFB3 enzyme as an imaging target, we used the new ^{18}F-radiolabeled PFKFB3-targeted ligand, [^{18}F]ZCDD083, which could be obtained in high radiochemical yields, activity concentrations and quality parameters. [^{18}F]ZCDD083 demonstrated high in vivo metabolic stability and long circulation time in the blood. The slow clearance from the blood may be explained by the high hydrophobicity of [^{18}F]ZCDD083. Indeed, a $LogD_{7.4}$ of 3.6 was reported for the parent compound AZ68.[16] The correlation of high hydrophobicity with high binding to plasma proteins and prolonged circulation time in the blood is well known.[28] High binding to plasma proteins is documented for the compound AZ26[16] (chemically similar to AZ68) and might be valid also for our tracer [^{18}F]ZCDD083. This may likely explain the slow tracer clearance. Also, the excretion route is usually related to lipophilicity, as lipophilic compounds are generally cleared via the hepatobiliary system. This is in accordance with our ex vivo biodistribution results which showed a predominant excretion from the liver to the intestines. We also noticed a high uptake in the lung. However, it is not clear whether this high uptake in the lung is due to nonspecific binding (due to the high [^{18}F]ZCDD083 lipophilicity) or somehow correlated with PFKFB3 tissue distribution. In 2003, Minchenko et al. studied the in vivo expression of the PFKFB enzyme family and its response to hypoxia, disclosing that lungs exhibit high basal level of PFKFB3 mRNA.[29] Moreover, the proteome analysis reported in the Human Protein Atlas shows that lung, stomach and placenta have the highest PFKFB3 expression among all tissues considered.[30]

Our PET imaging studies showed significantly increased signals in the aorta of ApoE$^{-/-}$ (+25%) and ApoE$^{-/-}$Fbn1$^{C1039G+/-}$ (+79%) compared to C57BL/6J mice. This is in accordance with the higher plaque burden in ApoE$^{-/-}$Fbn1$^{C1039G+/-}$ mice compared to ApoE$^{-/-}$ mice . Moreover, these results were supported by aortic autoradiography which showed a 2-fold increased uptake in the aortic arch of ApoE$^{-/-}$ compared to WT mice. The autoradiographic signal in ApoE$^{-/-}$Fbn1$^{C1039G+/-}$ was considerably higher too. The increment in uptake is clearly correlated with the increment in plaque load, as confirmed by histological evaluation. Indeed, the highest uptake was found

in ApoE$^{-/-}$Fbn1$^{C1039G+/-}$ at an advanced stage of the disease and high level of plaques in the aortic arch along with the thoracic aorta.

Unfortunately, despite the higher uptake, the [^{18}F]ZCDD083 signal in these small sized atherosclerotic plaques was affected by partial volume effect and due to the limited spatial resolution of PET[31] no “hotspots” could be detected in the in vivo imaging studies. Indeed, the vessel wall in mouse aorta is usually 30-80 µm, whereas the resolution in PET imaging is ~1,2 mm.[18]

The specificity of the tracer accumulation at the target structure (i.e. atherosclerotic plaque) was demonstrated by the combination of ex vivo autoradiography with en face Oil Red O staining of the same aortic specimens. Indeed, we observed co-localization of [^{18}F]ZCDD083 signal with plaque distribution along the aorta. These cross studies, involving C57BL/6J, ApoE$^{-/-}$ and ApoE$^{-/-}$Fbn1$^{C1039G+/-}$ demonstrated high sensitivity of [^{18}F]ZCDD083 to detect atherosclerotic plaques, whereas little signal was detected in normal vessel or outside atherosclerotic lesions. These stained areas exhibited a higher tracer accumulation. Hence, the [^{18}F]ZCDD083 uptake was clearly correlated with plaque distribution as well as with the progression of the disease.

Conclusion

In summary, we efficiently radiosynthesized a novel PET tracer, [^{18}F]ZCDD083 targeting the PFKFB3enzyme. Using in vivo and ex vivo studies, we characterized and validated [^{18}F]ZCDD083, demonstrating its ability to detect atherosclerotic plaques. This tracer may represent a promising tool for the non-invasive diagnosis and follow-up of atherosclerotic plaques prone to rupture, which in turn could help improving risk stratification and evaluation of the efficacy of anti-atherosclerotic therapies.

Currently, cardiovascular medicine aims principally to identify atherosclerotic plaques prone to rupture, improve the risk stratification, monitor the disease progression, assess new anti-atherosclerotic therapies and promptly evaluate the efficacy of therapeutic treatment. PET imaging is non-invasive and has a great potential in this context. Indeed, new targets and radiotracers are currently being investigated for imaging unstable atherosclerotic plaque.[6,7]

We have studied PFKFB3 enzyme as a new target to be used for the in vivo assessment of atherosclerotic plaques.[8,9] PFKFB3 is a glycolysis-related enzyme upregulated in inflammatory and hypoxic conditions.[10,11] Several studies have shown a tight correlation between PFKFB3 and angiogenesis, which is a feature of vulnerable atherosclerotic plaques.[12,13,14,15] Here we described the development of a specific PET radiotracer targeting PFKFB3 - the 18F-radiolabelled phenoxindazole ZCDD083 – based on the structure of the potent PFKFB3 inhibitor AZ68 (IC50= 4nM).[16]

Supporting Information

The Supporting Information is available on the ACS Publications website.

Author Contributions

CDD performed and co-designed all the experiments, contributed to writing the manuscript. SDA, and LW designed and performed radiochemistry experiments, corrected the manuscript. SS designed in vivo experiments and corrected the manuscript. GDM, and PP designed biology experiments and corrected the manuscript. MZ designed the experiments and wrote the manuscript.

Funding Sources

Acknowledgment

We thank the European Union's Horizon 2020 research and innovation programme under the Marie Skłodowska-Curie ITN-European Joint Doctorate MOGLYNET (grant agreement No. 675527).

Abbreviations

CCR2, CC chemokine receptor 2; CCL2, CC chemokine ligand 2; CCR5, CC chemokine receptor 5; TLC, thin layer chromatography.

References

1. Lusis, A. J. Atherosclerosis. *Nature* 407, 233–241 (2000).
2. Ross, R. Atherosclerosis — An Inflammatory Disease. *N. Engl. J. Med.* 340, 115–126 (1999).
3. Cardiovascular diseases (CVDs). Available at: https://www.who.int/news-room/fact-sheets/detail/cardiovascular-diseases-(cvds). (Accessed: 1st May 2019)
4. Roth, G. A. *et al.* Global, Regional, and National Burden of Cardiovascular Diseases for 10 Causes, 1990 to 2015. *J. Am. Coll. Cardiol.* 70, 1–25 (2017).
5. Spagnoli, L. G., Bonanno, E., Sangiorgi, G. & Mauriello, A. Role of Inflammation in Atherosclerosis. *J. Nucl. Med.* 48, 1800–1815 (2007).
6. Tawakol, A. & Finn, A. V. Imaging Inflammatory Changes in Atherosclerosis. *JACC Cardiovasc. Imaging* 4, 1119–1122 (2011).
7. Rudd James H.F., Hyafil Fabien & Fayad Zahi A. Inflammation Imaging in Atherosclerosis. *Arterioscler. Thromb. Vasc. Biol.* 29, 1009–1016 (2009).
8. Van Schaftingen, E., Jett, M. F., Hue, L. & Hers, H. G. Control of liver 6-phosphofructokinase by fructose 2,6-bisphosphate and other effectors. *Proc. Natl. Acad. Sci. U. S. A.* 78, 3483–3486 (1981).
9. Okar, D. A. & Lange, A. J. Fructose-2,6-bisphosphate and control of carbohydrate metabolism in eukaryotes. *BioFactors* 10, 1–14 (1999).
10. Pober, J. S. & Sessa, W. C. Evolving functions of endothelial cells in inflammation. *Nat. Rev. Immunol.* 7, 803–815 (2007).
11. Zhang, R., Li, R., Liu, Y., Li, L. & Tang, Y. The Glycolytic Enzyme PFKFB3 Controls TNF-α-Induced Endothelial Proinflammatory Responses. *Inflammation* 42, 146–155 (2019).
12. Tawakol, A. *et al.* HIF-1α and PFKFB3 mediate a tight relationship between pro-inflammatory activation and anaerobic metabolism in atherosclerotic macrophages. *Arterioscler. Thromb. Vasc. Biol.* 35, 1463–1471 (2015).
13. Parathath, S., Yang, Y., Mick, S. & Fisher, E. A. Hypoxia in murine atherosclerotic plaques and its adverse effects on macrophages. *Trends Cardiovasc. Med.* 23, 80–84 (2013).

14. Sluimer, J. C. & Daemen, M. J. Novel concepts in atherogenesis: angiogenesis and hypoxia in atherosclerosis. *J. Pathol.* 218, 7–29 (2009).
15. Perrotta, P. *et al.* Pharmacological strategies to inhibit intraplaque angiogenesis in atherosclerosis. *Vascul. Pharmacol.* 112, 72–78 (2019).
16. Boyd, S. *et al.* Structure-Based Design of Potent and Selective Inhibitors of the Metabolic Kinase PFKFB3. *J. Med. Chem.* 58, 3611–3625 (2015).
17. Qureshi, W. T., Rana, J. S., Yeboah, J., bin Nasir, U. & Al-Mallah, M. H. Risk Stratification for Primary Prevention of Coronary Artery Disease: Roles of C-Reactive Protein and Coronary Artery Calcium. *Curr. Cardiol. Rep.* 17, 110 (2015).
18. Vigne, J. *et al.* Current and Emerging Preclinical Approaches for Imaging-Based Characterization of Atherosclerosis. *Mol. Imaging Biol.* 20, 869–887 (2018).
19. Rathod, K. S., Hamshere, S. M., Jones, D. A. & Mathur, A. Intravascular Ultrasound Versus Optical Coherence Tomography for Coronary Artery Imaging – Apples and Oranges? *Interv. Cardiol. Rev.* 10, 8–15 (2015).
20. de Boer, S. P. M. *et al.* Determinants of high cardiovascular risk in relation to plaque-composition of a non-culprit coronary segment visualized by near-infrared spectroscopy in patients undergoing percutaneous coronary intervention. *Eur. Heart J.* 35, 282–289 (2014).
21. Hammad, B., Evans, N. R., Rudd, J. H. F. & Tawakol, A. Molecular imaging of atherosclerosis with integrated PET imaging. *J. Nucl. Cardiol.* 24, 938–943 (2017).
22. Skagen, K. *et al.* Carotid Plaque Inflammation Assessed with 18F-FDG PET/CT is Higher in Symptomatic Compared with Asymptomatic Patients. *Int. J. Stroke* 10, 730–736 (2015).
23. Tawakol, A. *et al.* In Vivo 18F-Fluorodeoxyglucose Positron Emission Tomography Imaging Provides a Noninvasive Measure of Carotid Plaque Inflammation in Patients. *J. Am. Coll. Cardiol.* 48, 1818–1824 (2006).
24. Joshi, N. V. *et al.* 18F-fluoride positron emission tomography for identification of ruptured and high-risk coronary atherosclerotic plaques: a prospective clinical trial. *The Lancet* 383, 705–713 (2014).

25. Rudd, J. H. F. *et al.* Imaging Atherosclerotic Plaque Inflammation by Fluorodeoxyglucose With Positron Emission Tomography. *J. Am. Coll. Cardiol.* 55, 2527–2535 (2010).
26. Emini Veseli, B. *et al.* Animal models of atherosclerosis. *Eur. J. Pharmacol.* doi:10.1016/j.ejphar.2017.05.010
27. Van der Donckt, C. *et al.* Elastin fragmentation in atherosclerotic mice leads to intraplaque neovascularization, plaque rupture, myocardial infarction, stroke, and sudden death. *Eur. Heart J.* 36, 1049–1058 (2015).
28. Gee, A. D., Bongarzone, S. & Wilson, A. A. Small Molecules as Radiopharmaceutical Vectors. in *Radiopharmaceutical Chemistry* (eds. Lewis, J. S., Windhorst, A. D. & Zeglis, B. M.) 119–136 (Springer International Publishing, 2019). doi:10.1007/978-3-319-98947-1_7
29. Minchenko, O., Opentanova, I. & Caro, J. Hypoxic regulation of the 6-phosphofructo-2-kinase/fructose-2,6-bisphosphatase gene family (PFKFB-1–4) expression in vivo. *FEBS Lett.* 554, 264–270 (2003).
30. Tissue expression of PFKFB3 - Summary - The Human Protein Atlas. Available at: https://www.proteinatlas.org/ENSG00000170525-PFKFB3/tissue. (Accessed: 2nd April 2019)
31. Position paper of the Cardiovascular Committee of the European Association of Nuclear Medicine (EANM) on PET imaging of atherosclerosis | SpringerLink. Available at: https://link.springer.com/article/10.1007%2Fs00259-015-3259-3. (Accessed: 5th February 2019)